Indian Journal of Chemical Technology
Vol. 30, September, 2023 pp. 656-666
DOI: 10.56042/ijct.v30i5.5210

# $Mn_3O_4$ and $Ag_2MnO_4$ nanoparticles loaded on *g*-$C_3N_4$ as magnetic catalysts for sonodegradation of dyes

Kaveh Parvanak Boroujeni[1]*, Farzaneh Keybandori[1] & Mohammad Mehdi Eskandari[2]

[1]Department of Chemistry, Shahrekord University, P. O. Box 88186-34141, Shahrekord, Iran
[2]Nanotechnology Research Center, Research Institute of Petroleum Industry, Tehran, Iran

*E-mail: parvanak-ka@sci.ac.ir

*Received 4 December 2022; accepted 19 April 2023*

New magnetic $Mn_3O_4$/*g*-$C_3N_4$ and $Ag_2MnO_4$/*g*-$C_3N_4$ nanocomposites have been synthesized based on Mn(II) Schiff base complex and used for sonodegradation of methylene blue (MB) and methyl orange (MO) dyes in aqueous solution. $Ag_2MnO_4$ nanoparticles (NPs) have been synthesized from $Mn_3O_4$ NPs and $AgNO_3$ under ultrasonic irradiation for the first time. The results indicate that the sonodegradation method of dyes in the presence of $Mn_3O_4$/*g*-$C_3N_4$ and $Ag_2MnO_4$/*g*-$C_3N_4$ nanocomposites is better than solar degradation processes. The better photodegradation rates for MB and MO dyes observed in the presence of $Ag_2MnO_4$/*g*-$C_3N_4$ (k= 0.0916 $min^{-1}$) and $Mn_3O_4$/*g*-$C_3N_4$ (k= 0.0381 $min^{-1}$), as compared to pure $Mn_3O_4$ and $Ag_2MnO_4$ compounds The synthesized nanocomposites are good fluorescent materials.

**Keywords:** Carbon nitride, Mn(II) Schiff base complex, Degradation of dyes, Sonochemistry

Graphitic carbon nitride (*g*-$C_3N_4$, GCN) is a two-dimensional organic polymer and it consists of s-triazine units. It is stable even at 600°C, and possesses a band gap of 2.7 eV. Since the discovery of GCN in 1834(Ref. 1), it has received much attention for their many potential applications in energy conversion, storage, photocatalytic systems, and environmental remediation[2]. Despite high efficiency, GCN suffers from some drawbacks such as fast recombination of photogenerated electron-hole pairs $e^-$-$h^+$, poor electrical conductivity, low visible-light absorption, and low surface area[3]. These shortcomings restrict their applications especially in photocatalytic systems. One strategy is coupling with some metal oxides (as suitable semiconductors) such as $TiO_2$, $Zn_2GeO_4$, $SmVO_4$, $Ag_2O$, $Fe_2O_3$, and Pt/$TiO_2$/$MnO_x$. It is a feasible route to enhance charge separation, lower the recombination rate and improve the photocatalytic performance[4,5]. Among all metal oxides, manganese oxide nanoparticles (NPs) have gained much attention in electronics and optoelectronic fields due to the high surface area and their wide band gap energy[6,7]. To the best of our knowledge, there has been no report in the literature on the coupling of $Mn_3O_4$ nanomaterials with GCN.

With huge industrialization, a larger number of hazardous pollutants have been released to the environment which poses a threat to the health of humans and other animals. Among these, organic dyes are one of the major pollutant factors of water and environment. Nowadays, researchers try to find a low cost and effective method for removal of dyes such as coagulation, flocculation, reverse osmosis, ultrafiltration, and adsorption[8]. However, the generation of a secondary waste product which cannot be further destroyed is still one of the majorly drawbacks. To solve this problem, the attention was focused on semiconductor-mediated photocatalytic degradation reactions, in which photogenerated electron-hole pairs arising from redox reactions yield active radical species that cause degradation of dye without production of waste byproducts. Based on this concept, various photocatalysts have been designed and tested for the degradation of dyes[9].

In continuation of the studies on synthesis of new NPs[10,11], herein, we want to report the synthesis of $Mn_3O_4$/*g*-$C_3N_4$ and $Ag_2MnO_4$/*g*-$C_3N_4$ nanocomposites and their applicability as magnetically catalysts for sonodegradation of MB and MO dye pollutants. It was hoped that incorporation of these manganese oxide into the *g*-$C_3N_4$ matrix improves its photoactivity properties, and hence it can act as a hybrid organic/inorganic semiconductor with future perspectives for nanodevices.

## Experimental Section

### Chemicals and characterization techniques

Ultrasonic generator was carried out on ultrasonic probe (Top- Sonics UPH-400, ultrasonic technology development Co.). Fourier transform infrared (FT-IR) spectra were recorded on a Schimadzu system FT-IR 8400 spectrophotometer using KBr pellets. Product X-ray diffraction (XRD) data were recorded by a Rigaku D-max C III, X-ray diffractometer using Ni-filtered Cu-Kα radiation. Field emission scanning electron microscope (FE-SEM) images were recorded by a Hitachi s4160/Japan with gold coating that was coupled with a link energy dispersive X-ray (EDX) analyzer. Electronic spectra of the compounds were recorded using Cary 50 spectrophotometer. The samples for UV-visible measurements were well dispersed in ethanol by sonication for 25 min, to obtain a homogeneous suspension. The magnetic properties of the samples were measured at room temperature (298 K) using a vibrating sample magnetometer (VSM, MDKFD, Meghnatis Kavir Kashan Co., Kashan, Iran). Fluorescence spectra were recorded on a Cary eclipse spectrofluorometer at room temperature.

### Synthesis of $H_2L$ Schiff base Ligand

The *N*,*N*'-di(5-bromosalicylidene)-*o*-phenylenediamine ligand was synthesized according to previously reported procedure[11,12].

### Synthesis of [Mn(L)(MeOH)$_2$] complex

For synthesis of dimethanol-*N*,*N*'-phenylene-bis(5-bromosalicylideneaminato)manganese(II) complex, 5 mL methanolic solution of $H_2L$ (0.047 g, 0.1 mmol) was added drop wise to a methanolic solution of $Mn(CH_3COO)_2.4H_2O$ (0.0173 g, 0.1 mmol) under ultrasonic irradiation (250 W). The mixture was then exposed to ultrasonic irradiation for 20 min. After filtration, the formed brown precipitate was gathered and well washed with cold methanol and ether (10 mL). The final powder was obtained after drying over anhydrous $CaCl_2$ under vacuum (Yield 75%, $T_{mp}$> 300ºC).

### Synthesis of $Mn_3O_4$ NPs

In order to synthesis of $Mn_3O_4$ NPs, the [Mn(L)(MeOH)$_2$] complex as a new precursor was placed in an electronic furnace (400ºC ) which decomposes to form NPs after 1 h. The obtained NPs were cooled to room temperature, washed successively with water and ethanol (10 mL), and air-dried.

### Synthesis of $Ag_2MnO_4$ NPs

For synthesis of $Ag_2MnO_4$ NPs, 0.228 g (1 mmol) of $Mn_3O_4$ NPs were suspended in 50 mL water and then 0.338 g (2 mmol) of $AgNO_3$ was added to this mixture, slowly. The mixture was exposed to ultrasonic irradiation (250 W) for 30 min. The pH was adjusted to 7 by NaOH (1M). Afterwards, the above mixture was stirred at dark condition for 7 h. The black precipitation was centrifuged, washed with water and ethanol several times (3 × 10 mL), and air-dried.

### Synthesis of *g*-$C_3N_4$ powder

Mesoporous carbon nitride (MCN) was prepared using SBA-15 nanorod as a template according to our previous report[13].

### Synthesis of $Mn_3O_4$/*g*-$C_3N_4$ and $Ag_2MnO_4$/*g*-$C_3N_4$ nanocomposites

To 10 mL ethanolic suspension of the *g*-$C_3N_4$ (0.0001 g) was added drop wise 10 mL ethanolic suspension of the $Mn_3O_4$ (0.1 g, 0.4 mmol) or $Ag_2MnO_4$ (0.1 g, 0.3 mmol). The mixture was refluxed at 90ºC for 30 min and exposed to ultrasonic irradiation (200 W) for 10 min. The prepared powder was separated by centrifuge, washed rigorously with water and ethanol (15 mL), and dried at 120ºC overnight.

### Photocatalytic experiment

The photocatalytic activity of the $Mn_3O_4$/*g*-$C_3N_4$ and $Ag_2MnO_4$/*g*-$C_3N_4$ nanocomposites was tested by the removal of methylene blue (MB) or methyl orange (MO) as organic dyes in aqueous solutions under solar and ultrasound irradiation. In the first step, degradation process of dyes was investigated under solar irradiation. First, the dosage of photocatalyst (0.003–0.005 mg), amount of $H_2O_2$ (0–5 mL), and pH of the solution (5–10) were selected and optimized. The photocatalytic tests were performed on the days (10 a.m. to 2 p.m.) of bright sunny light (average light intensity of 180 mW cm$^{-2}$). Typically, 0.005 g of the sample as photocatalyst was added to 50 mL of MB or MO aqueous solution (5 mg/L) and the mixture were stirred (500 rpm) at room temperature in the dark for 30 min. In dark condition, adsorption$^{-1/n}$ desorption equilibrium between dye and catalyst was established. Then, the mixture was exposed to solar light in the presence of an appropriate amount of $H_2O_2$ (30%) at suitable pH, and consequently the dye degradation process took place. At determined time intervals, 3 mL of the mixture was centrifuged and the photocatalyst was separated. Degradation process of

each dye was checked by measuring the absorptions of MB and MO at 663 and 462 nm, respectively, on each UV-visible spectrum. Degradation of dyes under ultrasound irradiation (250 W) was accomplished in a similar manner. The pH of solutions can be easily adjusted by adding NaOH (1 M) or HCl (1 M). The percent of degradation was calculated according to the following equation:

*Degradation (%)* = $(C_o - C_t)/C_o \times 100$, where $C_o$ is the initial concentration and $C_t$ is the concentration after the determined time (t).

## Results and Discussion

For preparation of $Mn_3O_4/g\text{-}C_3N_4$ and $Ag_2MnO_4/g\text{-}C_3N_4$ nanocomposites, first the Mn(II)complex ($Mn(L)(MeOH)_2$) as a new precursor was synthesized based on Schiff base ligand ($H_2L$), prepared from 1,2-diaminocyclohexane and 5-bromosalicylaldehyde (Scheme 1). In the second step, $Mn_3O_4$ NPs were prepared via solid-state thermal decomposition of this precursor. In the third step, $Ag_2MnO_4$ NPs were synthesized from the obtained $Mn_3O_4$ NPs in the presence of $AgNO_3$under ultrasonic irradiation. To the best of our knowledge, this is the first time that such strategy is used to synthesize $Ag_2MnO_4$ NPs. Finally, $Mn_3O_4/g\text{-}C_3N_4$ and $Ag_2MnO_4/g\text{-}C_3N_4$ nanocomposites were prepared from the interaction of $Mn_3O_4$ NPs or $Ag_2MnO_4$ NPs with $g\text{-}C_3N_4$ in the presence of ultrasonic irradiation.

Fig. 1 shows XRD patterns of $Mn_3O_4$ and $Ag_2MnO_4$ compounds, respectively. The XRD plot of $Mn_3O_4$ displays the diffraction peaks of $Mn_3O_4$ phase (JCPDS Card No. 75-1560) with tetragonal phase (Space group: I41/amd, No: 141). The crystallographic parameters of a, b, and c parameters are 5.762, 5.762 and 9.439Å, respectively. Also, values of α, β, and γ parameters are 90.00°. The significant peaks of $Mn_3O_4$ phase are observed at 2θ = 29.01º, 32.50º, and 36.26º which can be perfectly related to (112), (103), and (211) crystal planes,

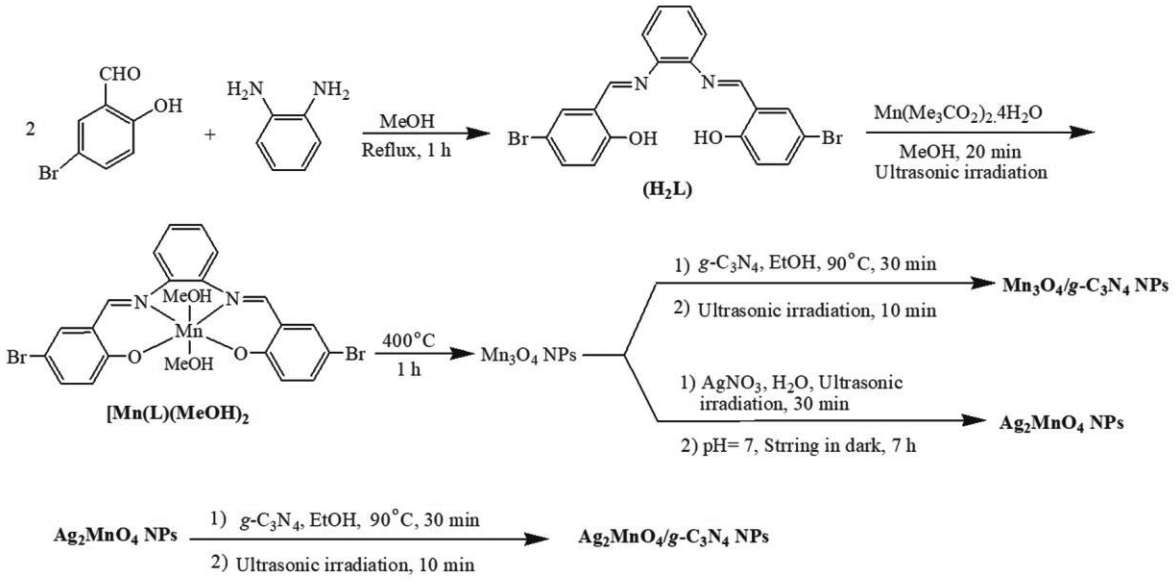


Scheme 1 — Multi-step synthesis of$Mn_3O_4/g\text{-}C_3N_4$ and $Ag_2MnO_4/g\text{-}C_3N_4$ nanocomposites

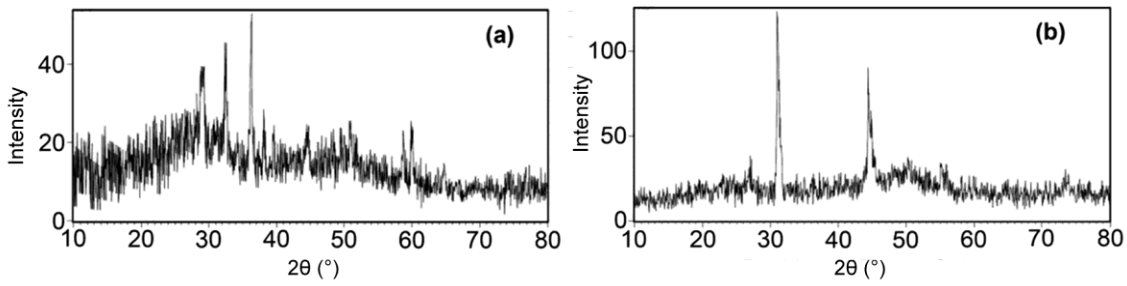


Fig. 1 — XRD patterns of (a) synthesized $Mn_3O_4$ and (b) $Ag_2MnO_4$ (2)

respectively. The XRD plot of $Ag_2MnO_4$ shows pattern of $Ag_2MnO_4$ phase (JCPDS Card No. 76-1584) with orthorhombic phase (Space group: Pnma, No: 62). The parameter values of a, b, and c are 9.998, 6.989 and 5.474 Å, respectively. The peaks appeared at 31.04º and 44.53º are related to (301) and (420) planes. The XRD patterns show small size of the $Mn_3O_4$ and $Ag_2MnO_4$ particles due to wide width of the diffraction peaks. The mean sizes of the $Mn_3O_4$ and $Ag_2MnO_4$ particles were calculated to be 22.83 and 41.85 nm, respectively by the Debye–Scherrer equation[14].

FT-IR spectra of the nano-sized of $[Mn(L)(MeOH)_2]$ complex precurser, the $Mn_3O_4$/*g*-$C_3N_4$ and $Ag_2MnO_4$/*g*-$C_3N_4$ nanocomposites, are shown in Fig. 2. In Fig. 2a, the sharp band at 1607 $cm^{-1}$ is related to C=N group. This peak exhibits a red shift to lower frequency toward the ligand $H_2L$ (1628 $cm^{-1}$)[12], indicating that the ligand is coordinated to the Mn ions via the nitrogen atoms of the azomethine groups. The appearance of bands in the range of 400–500 $cm^{-1}$, due to metal-oxygen and metal-nitrogen vibration frequencies, confirms the complex formation[15]. FT-IR spectra of the $Mn_3O_4$/*g*-$C_3N_4$ and $Ag_2MnO_4$/*g*-$C_3N_4$ nanocomposites are given in Figs. 2b and c, respectively. It is clear that frequencies of complex precursor were diminished. The peaks at about 1607, 2900, and 3430 $cm^{-1}$areduo to C=N, C–H, and N–H bonds of *g*-$C_3N_4$ support[13,16]. The bands in the region of 1100–1400 $cm^{-1}$ and ~ 700 $cm^{-1}$are assigned to the typical stretching frequencies of the C–N bond of heterocyclic rings and the out-of-plane bending vibration of the s-triazine rings of *g*-$C_3N_4$[13,16], respectively. The bands in the region of ~ 500 $cm^{-1}$ are corresponded to the Mn–O bonds[17]. The broad peaks located at ~3400 $cm^{-1}$ are assigned to O–H bonds of adsorbed water in the KBr tablet or sample[11].

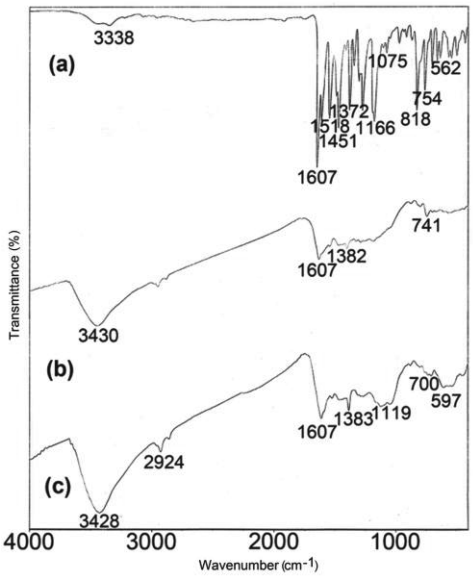


Fig. 2 — FT-IR spectra of (a) $[Mn(L)(MeOH)_2]$ complex, (b) $Mn_3O_4$/*g*-$C_3N_4$, and (c) $Ag_2MnO_4$/*g*-$C_3N_4$ nanocomposites

The morphologies of the obtained $Mn_3O_4$/*g*-$C_3N_4$ and $Ag_2MnO_4$/*g*-$C_3N_4$ nanocomposites were investigated by FE-SEM analysis (Figs. 3a and b), revealing that they have the spherical structures. The particle size distribution of $Mn_3O_4$/*g*-$C_3N_4$ and $Ag_2MnO_4$/*g*-$C_3N_4$ nanocomposite were found to be 16–20 and 21–25 nm, respectively (Figs. 3c and d), which are smaller in size in comparison to that achieved for $Mn_3O_4$ and $Ag_2MnO_4$ (Fig. 1), due to benefits of applying ultrasonic irradiation during the synthetic processes.

EDX spectra of the $Mn_3O_4$/*g*-$C_3N_4$ and $Ag_2MnO_4$/*g*-$C_3N_4$ nanocomposites are given in Fig. 4. The spectrum of $Mn_3O_4$/*g*-$C_3N_4$nanocomposite (Fig. 4a) exhibited Mn, O, N, and C signals, only. Also, the spectrum of $Ag_2MnO_4$/*g*-$C_3N_4$ nanocomposite merely showed Mn, Ag, O, N, and C signals. Quantitative results are given in a Table inserted in the corresponding the figures. The Si signal appeared at around 1.5 KeV is duo to the coating material of the instrument[10].

The variation in magnetization (M) vs. applied field (H) for $Mn_3O_4$/*g*-$C_3N_4$ and $Ag_2MnO_4$/*g*-$C_3N_4$ nanocomposites at 298 K are plotted in Fig. 5. The hysteresis loop shows a superparamagnetic behaviour of the sample. The values of saturation magnetization ($M_s$) for $Mn_3O_4$/*g*-$C_3N_4$ and $Ag_2MnO_4$/*g*-$C_3N_4$ nanocomposites are about 0.046 and 0.067 emu/g, respectively.

The electronic properties of the prepared compounds were surveyed by UV–visible spectroscopy (Fig. 6a). The absorbance spectrum of the $Mn_3O_4$ indicated the bands at around 200–300 and 400–500 nm, which are related to $O^{2-} \rightarrow Mn^{2+}$ and $O^{2-} \rightarrow Mn^{3+}$ charge transfer transitions, respectively[18]. Also, the band at 640 nm can be related to d–d crystal field transitions, $^3E_g(G) \leftarrow {}^3T_{1g}$, $^3A_{2g}(F) \leftarrow {}^3T_{1g}$, $^3A_{2g}(G) \leftarrow {}^3T_{1g}$, $^3T_{2g}(H) \leftarrow {}^3T_{1g}$, $^3T_{1g}(H) \leftarrow {}^3T_{1g}$, and $^3E_g(H) \leftarrow {}^3T_{1g}$ on octahedral $Mn^{3+}$ions[19]. The spectrum of the $Ag_2MnO_4$ show the bands at 200–300 nm, related to $O^{2-} \rightarrow Mn^{6+}$ charge transfer transitions in the $MnO_4^{2-}$groups[20]. Fig. 6b shows curve of $(Ah\upsilon)^2$ *vs.* hυ for the synthesized compounds. The

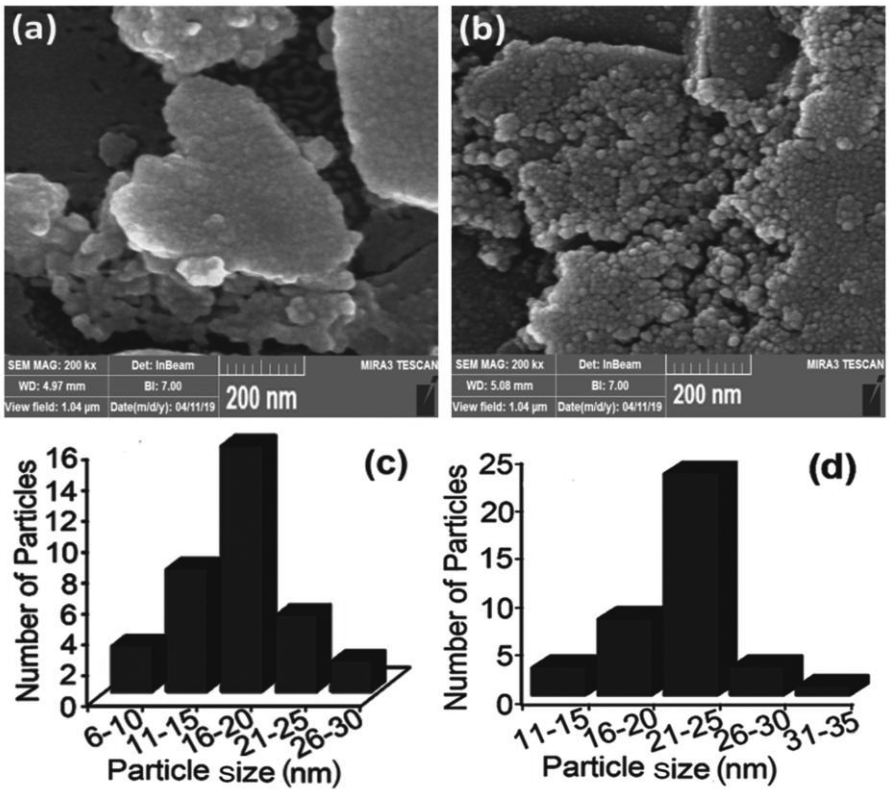


Fig. 3 — FE-SEM images of the $Mn_3O_4$/*g*-$C_3N_4$ (a) and $Ag_2MnO_4$/*g*-$C_3N_4$ (b) nanocomposites and their particle size distribution (c and d, respectively)

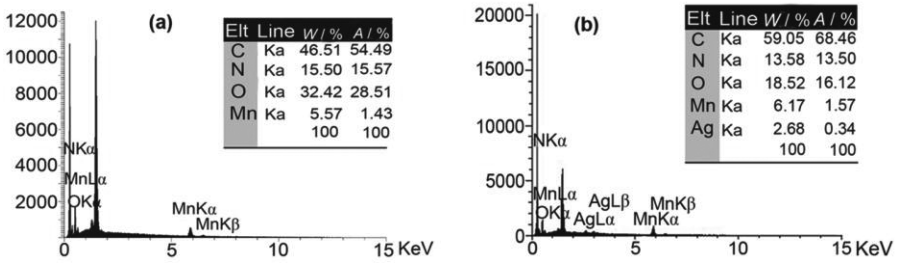


Fig. 4 — EDX spectra of the $Mn_3O_4$/*g*-$C_3N_4$ (a) and $Ag_2MnO_4$/*g*-$C_3N_4$ (b) nanocomposites

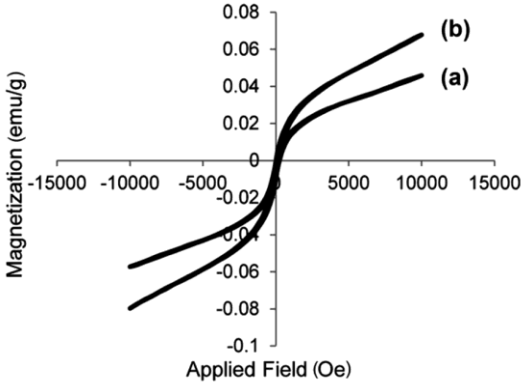


Fig. 5 — VSM analysis of (a) $Mn_3O_4$/*g*-$C_3N_4$ and (b) $Ag_2MnO_4$/*g*-$C_3N_4$ nanocomposites at 298 K

band gap ($E_g$) can be surveyed by the $(Ah\upsilon)^2 = B\ (h\upsilon\text{-}E_g)$ formula[21], where hυ, A and B are the photon energy, absorption coefficient and a constant duo to the material type. By extrapolation of the corresponding curves the $E_g$ values of $Mn_3O_4$, $Ag_2MnO_3$, $Mn_3O_4$/*g*-$C_3N_4$ and $Ag_2MnO_4$/*g*-$C_3N_4$ are estimated to be 2.6, 3.6, 2.2 and 3.7eV, respectively. The fluorescence bands of the synthesized compounds were surveyed when excited at wavelength of 334 nm at room temperature (Fig. 6c). The fluorescence emission bands of $Mn_3O_4$, $Ag_2MnO_3$, $Mn_3O_4$/g-$C_3N_4$, and $Ag_2MnO_3$/*g*-$C_3N_4$ are located at 448, 451, 450, and 437 nm, respectively. As it can be seen, the intensity fluorescence peaks of the $Mn_3O_4$/*g*-$C_3N_4$ and $Ag_2MnO_3$/*g*-$C_3N_4$ samples are enhanced as compared

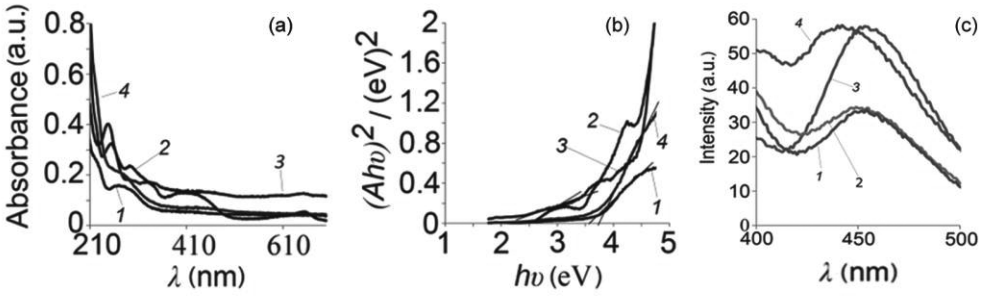


Fig. 6 — Electronic spectra of the synthesized compounds (a), their corresponding $(Ah\upsilon)^2$–$h\upsilon$ curves (b), and their corresponding fluorescence spectra at excitation wavelength of 334 nm at room temperature, $Ag_2MnO_4$ (1), $Mn_3O_4$ (2), $Mn_3O_4$/*g*-$C_3N_4$ (3), $Ag_2MnO_4$/*g*-$C_3N_4$ (4)

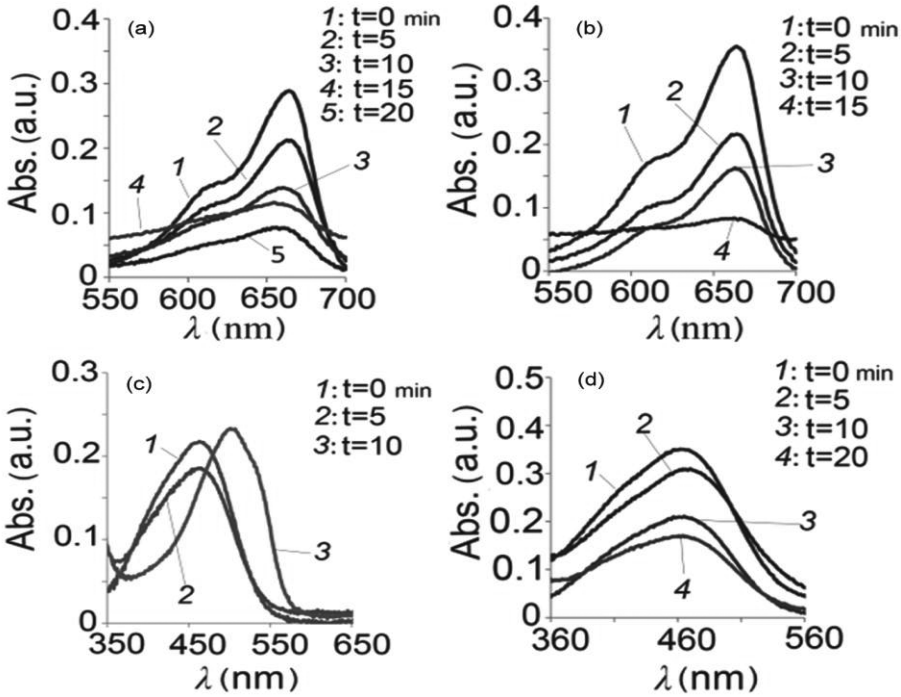


Fig. 7 — Time related absorption spectra during sonodegradation process of MB and MO dyes over the $Mn_3O_4$/*g*-$C_3N_4$ (a,c, respectively) and $Ag_2MnO_4$/*g*-$C_3N_4$ (b,d, respectively) nanocomposites

to that of the corresponding samples without of *g*-$C_3N_4$. Clearly, the present of the *g*-$C_3N_4$ support has caused higher intensity with a slight shift of wavelength. It is well known that the *g*-$C_3N_4$ derivatives, consisting of powerful fluorescence emission bands, have been used in various fields such as in fluorescent sensors, biosensor, fluorescence probes, photocalorimetry, and cancer therapy[22]. Likewise, according to our investigation the prepared $Mn_3O_4$/*g*-$C_3N_4$ and $Ag_2MnO_3$/*g*-$C_3N_4$ nanocomposites are predicted to be eco-friendly applicable industrial compounds.

The photocatalytic activities of the synthesized compounds for degradation of MB and MO dyes were investigated at room temperature in aqueous solution. Firstly, the degradation process was carried out for MB dye (cationic dye). The degradation of MB dye was surveyed at 664 nm, showing the characteristic absorption. The absorption bands in different time under optimized conditions (pH=7, $[H_2O_2]$=1mL, $[Mn_3O_4/g\text{-}C_3N_4]$=3 mg, [MB]=4 mg/L) have been shown in Fig. 7a. The characteristic absorption declines for a period of time (20 min) under ultrasonic irradiation. Also, the absorption spectrum under

another optimized conditions (pH=5, [$H_2O_2$]=2 mL, $Ag_2MnO_4$/*g*-$C_3N_4$= 3 mg, [MB]=4 mg/L) in a shorter period time (15 min) under ultrasonic irradiation has been displayed in Fig. 7b. The absorption of MB dye is close to zero after the period of irradiation times as the intense blue colour of the solution is decreased, indicating the progression of dye degradation. Clearly, the characteristic absorption band of MB at 664 nm was not shifted, showing the degradation of dye is related to destruction of chromophore groups[23]. The efficiencies of degradation of MB dye over the $Mn_3O_4$/*g*-$C_3N_4$ and $Ag_2MnO_4$/*g*-$C_3N_4$ nanocomposite were determined to be 96 (in 20 min) and 78% (in 15 min), respectively. However, 22 and 4% of the dye was destroyed over $Mn_3O_4$/*g*-$C_3N_4$ and $Ag_2MnO_4$/*g*-$C_3N_4$ nano-composites, respectively, in dark condition. Under solar light, dye degradation efficiency using $Mn_3O_4$/*g*-$C_3N_4$ and $Ag_2MnO_4$/*g*-$C_3N_4$ nanocomposites were found to be 87 (in 30 min) and 81% (in 50 min), respectively. The degradation efficiency of dye under solar light in the presence of $Mn_3O_4$ and $Ag_2MnO_4$were estimated to be 83 (in 50 min) and 84% (in 60 min), respectively. Likewise, the photocatalytic activity of the synthesized compounds was investigated for degradation of MO dye (anionic dye) under similar conditions. The intensity alterations of the bands at 462 nm over the $Mn_3O_4$/*g*-$C_3N_4$ and $Ag_2MnO_4$/*g*-$C_3N_4$ nanocomposites under ultrasonic irradiation at different times are depicted in Figs. 7c and d, respectively. The efficiency of degradation of MO dye was estimated to be 60% after 5 min over $Mn_3O_4$/*g*-$C_3N_4$under optimized conditions (pH=7, [$H_2O_2$]=2 mL, [$Mn_3O_4$/*g*-$C_3N_4$]= 0.005 g and [MO]= 3 mg/L). Also, dye degradation efficiency was 29 % after 20 min over $Ag_2MnO_4$/*g*-$C_3N_4$ nano-composite under optimized conditions (pH=6, [$H_2O_2$]=0 mL, [$Ag_2MnO_4$/*g*-$C_3N_4$]= 0.005 g and [MO]= 5 mg/L).The efficiencies of degradation of MO dye were obtained to be 78% after 40 min and 28% after 30 min over $Mn_3O_4$/*g*-$C_3N_4$ and $Ag_2MnO_4$/*g*-$C_3N_4$ nanocomposites under solar light, respectively. The obtained results summarized in Table 1. Based on the above results, the prepared nanocomposites seem to be slightly preferable for sonodegradation of MB and MO dyes for the desired efficiency at shorter times.

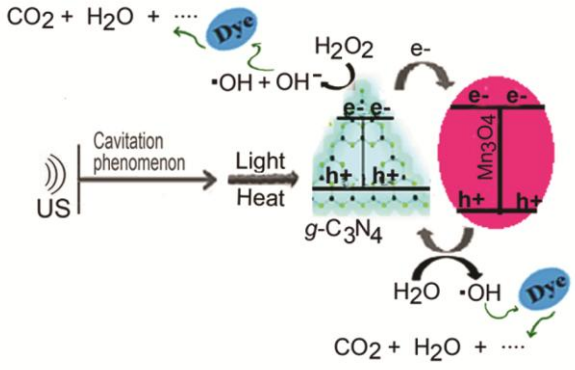


Fig. 8 — Proposed mechanism of dye degradation under ultrasonic irradiation in aqueous solution over $Mn_3O_4$/*g*-$C_3N_4$ nanocomposites

A proposed mechanism for the degradation of MB or MO dyes over $Mn_3O_4$/*g*-$C_3N_4$ nanocomposite under ultrasonic light is given below in Fig. 8. The cavitation phenomenon can happen in a liquid medium in the presence of ultrasonic irradiation which consists of generation, growth, and collapse of bubbles with low lifetime (a few microseconds). Over the course of this occurrence the relatively wide wavelength range of light can be produced (sonoluminescence), resulting in the creation of high local pressure and temperature[24]. In this condition, *g*-$C_3N_4$ under an excitation wavelength produces electron-hole pairs (Eq. (1)). $H_2O_2$ molecules react with the electrons on the CB (conductive band), leading to the formation of •OH radical groups (Eq. (2)). Electrons transfer from *g*-$C_3N_4$ to the $Mn_3O_4$NPsoccurs and reversible holes are transferred from $Mn_3O_4$ to *g*-$C_3N_4$, which impede the recombination of electron-hole pairs. This process

Table 1 — Degradation of MB[1] and MO[2] dyes in the presence of the synthesized compounds

| Photocatalyst | Irradiation | D.E.[a] (at dark, %) | D.E. (under irradiation, %) | Total D.E. (%) | Degradation time (min) | Rate constant ($min^{-1}$) |
|---|---|---|---|---|---|---|
| $Mn_3O_4$ | Solar | 18[1],45[2] | 65[1],33[2] | 83[1],78[2] | 50[1],50[2] | 0.0181[1], 0.0075[2] |
| $Mn_3O_4$/*g*-$C_3N_4$ | Solar | 22[1],43[2] | 65[1],35[2] | 87[1],78[2] | 30[1],40[2] | 0.0373[1], 0.0123[2] |
| $Mn_3O_4$/*g*-$C_3N_4$ | Ultrasound | 22[1], 43[2] | 74[1],17[2] | 96[1],60[2] | 20[1],5[2] | 0.0673[1], 0.0381[2] |
| $Ag_2MnO_4$ | Solar | 15[1],0.5[2] | 69[1],26[2] | 84[1],26.5[2] | 60[1],40[2] | 0.0206[1], 0.0082[2] |
| $Ag_2MnO_4$/*g*-$C_3N_4$ | Solar | 4[1],4[2] | 77[1],24[2] | 81[1],28[2] | 50[1],30[2] | 0.0258[1], 0.0089[2] |
| $Ag_2MnO_4$/*g*-$C_3N_4$ | Ultrasound | 4[1],4[2] | 74[1],25[2] | 78[1],29[2] | 15[1],20[2] | 0.0916[1], 0.0136[2] |

[a]Degradation efficiency

could effectively improve the separation efficiency of the sonogenerated electron-hole pair and the lifetime of the excited electron-hole pair. In addition, the interaction of holes on the VB (valence band) with water molecules provides more •OH radicals (Eq. (3)). The generated •OH radicals destroy the structure of dyes to $H_2O$, $CO_2$ and other inorganic products (Eq. (4)). Therefore, as mentioned above, shorter reaction time in sonodegradation processes using the synthesized nanocomposites is probably due to the fast generation and separation of electron and hole pairs, producing more amounts of the active OH radicals. Meanwhile, sonication of a liquid medium also leads to the generation of radicals ($H_2O \rightarrow •H + •OH$). Although, the $H_2O_2$ molecules are helpful to improve dye degradation efficiency, through producing more active •OH radicals, but no increase of the rate of degradation process could be observed after a critical concentration of $H_2O_2$[25]. It's necessary to mention that, the boosted sonocatalytic activity of $Mn_3O_4/g\text{-}C_3N_4$ and $Ag_2MnO_4/g\text{-}C_3N_4$ nanocomposites can be also attributed to the present of $g\text{-}C_3N_4$ with a strong-coupling interface, allowing a rapid transfer of the generated electron-hole pairs.

$$g\text{-}C_3N_4 + \text{ultrasonic irradiation} \rightarrow h^+_{VB} + e^-_{CB} \quad \ldots (1)$$

$$H_2O_2 + e^-_{CB} \rightarrow •OH + OH^- \quad \ldots (2)$$

$$H_2O/OH^- + h^+_{VB} \rightarrow •OH + H^+ \quad \ldots (3)$$

$$\text{Organic dye} + •OH \rightarrow H_2O, CO_2, NO_3^-, SO_4^{2-}, \quad \ldots (4)$$

The degradation kinetics of MB and MO dye over the synthesized compounds were investigated and presented in Fig. 9. Kinetic data fitted well with pseudo-first-order model and it is described by the following equation: $LnC_t = -kt + LnC_0$, where $C_0$ is the dye concentration in initial moment, $C_t$ is concentration after irradiation (solar or ultrasonic), k is the rate constant of reaction, and t is the reaction time. Figs. 9a and b show the k values for the degradation of MB dye in the presence of ultrasonic irradiation, to be 0.0673 and 0.0916 $min^{-1}$ over $Mn_3O_4/g\text{-}C_3N_4$ and $Ag_2MnO_4/g\text{-}C_3N_4$ nanocomposites, respectively. For the case of MO dye the k values were obtained to be 0.0381 and 0.0136 $min^{-1}$ in the presence of $Mn_3O_4/g\text{-}C_3N_4$ and $Ag_2MnO_4/g\text{-}C_3N_4$ nanocomposites, respectively (Figs. 9c and d). With comparison of the obtained results from sonocatalytic degradation of dyes over the synthesized nanocomposites, it is clear that MB and MO dyes are destroyed with higher rate constant in the presence of $Ag_2MnO_4/g\text{-}C_3N_4$and $Mn_3O_4$/g-$C_3N_4$nanocomposites, respectively (Fig. 10). The dye degradation kinetics verified that both

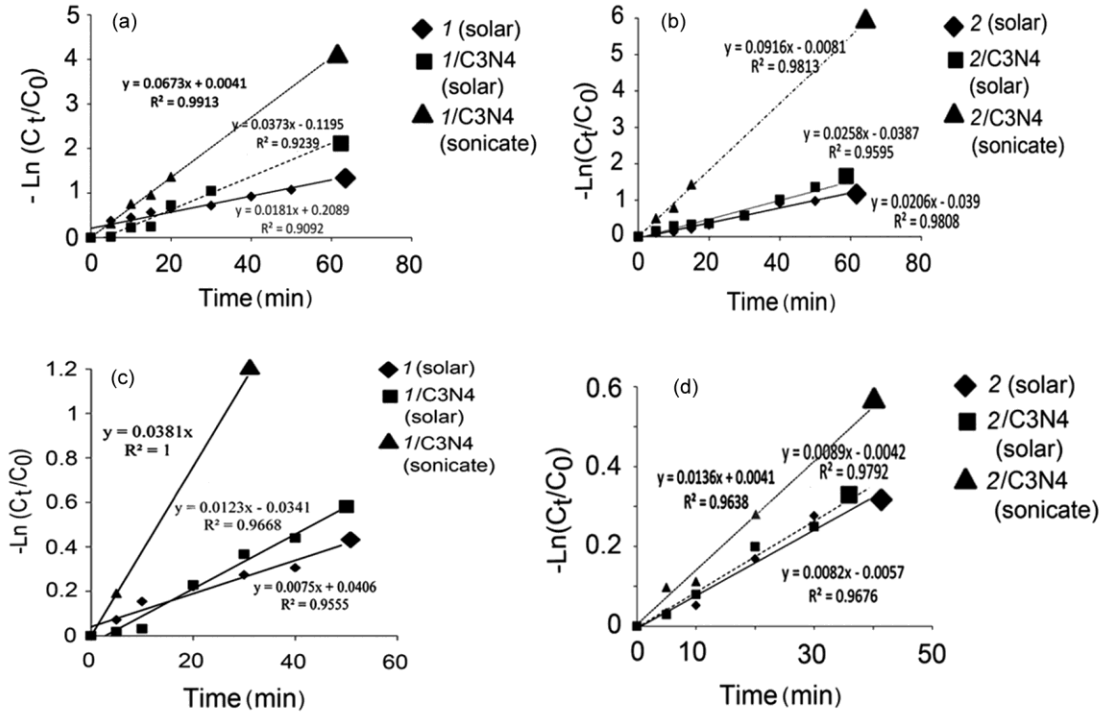


Fig. 9 — Degradation kinetics of MB (a, b) and MO (c, d) dyes over the synthesized compounds; $Mn_3O_4$ (1) and $Ag_2MnO_4$ (2)

Table 2 — Comparison of degradation of MB and MO dyes over different nanomaterials

| Nanomaterial | Irradiation | Cat. (mg) | Dye (mg/L) | Dye | Degradation Efficiency (%) | Time (min) |
|---|---|---|---|---|---|---|
| $Ag/TiO_2$ | Solar | 50 | 7.5 | MO | 65.4 | 120[26] |
| $Zn_3(PO_4)_2@C_3N_4$ | Visible | 30 | 20 | MB | 90 | 280[27] |
| $Zn_3(VO_4)_2/g\text{-}C_3N_4$ | Visible | 50 | 10 | MB | 95.45 | 300[28] |
| CdS/RGO/CNT[a] | Visible | 20 | 10 | MB | 62 | 30[29] |
| $ZnFe_2O_4$ | Microwave | 60 | 1 | MB | 32 | 30[30] |
| Tl0.6-$Mn_3O_4$[b] | Heat | 5 | 5 | MB | 76.9 | 30[31] |
| $Mn_3O_4$ | UV | 100 | $5\times10^{-5}$ | MB | 26 | 120[32] |
| $Mn_3O_4$ | UV | 100 | $5\times10^{-5}$ | MO | 26 | 120[32] |
| MIL-101(Cr)/RGO/$ZnFe_2O_4$ | Ultrasound | 500 | 25 | MO | 80 | 70[33] |
| $Mn_3O_4$ nanorods | Heat | 10 | 100 | MB | 95 | 60[34] |
| $Mn_3O_4/g\text{-}C_3N_4$ | Ultrasound | 3 | 4 | MB | 96 | 20 |
| $Mn_3O_4/g\text{-}C_3N_4$ | Ultrasound | 5 | 3 | MO | 60 | 5 |
| $Ag_2MnO_4/g\text{-}C_3N_4$ | Ultrasound | 3 | 4 | MB | 78 | 15 |
| $Ag_2MnO_4/g\text{-}C_3N_4$ | Ultrasound | 5 | 5 | MO | 29 | 20 |

[a] RGO: Reduced graphene oxide, CNT: Carbon nanotube
[b] Thallium doped $Mn_3O_4$

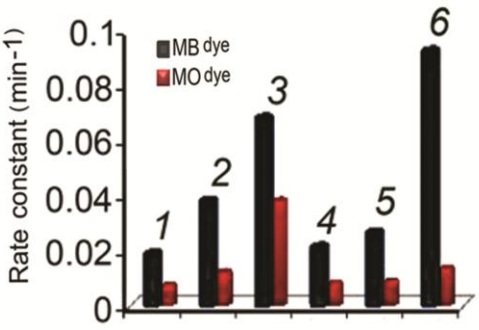


Fig. 10 — Rate constant of MB and MO dyes over the synthesized compounds, $Mn_3O_4$, solar irradiation (1), $Mn_3O_4/g\text{-}C_3N_4$, solar irradiation (2), $Mn_3O_4/g\text{-}C_3N_4$, sonication (3), $Ag_2MnO_4$, solar irradiation (4), $Ag_2MnO_4/g\text{-}C_3N_4$, solar irradiation (5), $Ag_2MnO_4/g\text{-}C_3N_4$, sonication (6)

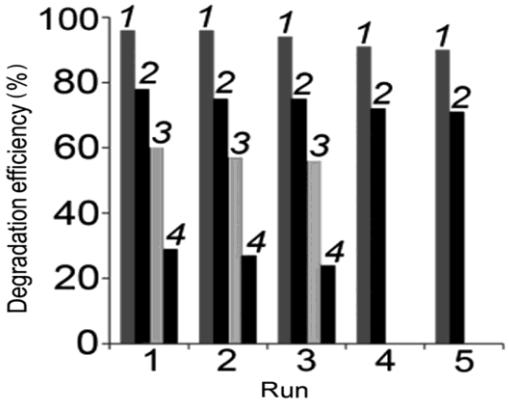


Fig. 11 — Successive recycle runs of nanocomposites for sonodegradation of dyes, $Mn_3O_4/g\text{-}C_3N_4$, MB (1), $Ag_2MnO_4/g\text{-}C_3N_4$, MB (2), $Mn_3O_4/g\text{-}C_3N_4$, MO (3), $Ag_2MnO_4/g\text{-}C_3N_4$, MO (4)

$Ag_2MnO_4/g\text{-}C_3N_4$ and $Mn_3O_4/g\text{-}C_3N_4$ nanocomposites are more superior in photodegradation of dyes compared to their unsupported counterparts, $Ag_2MnO_4$ and $Mn_3O_4$. Thus, we concluded that the presence of both $g\text{-}C_3N_4$ and ultrasonic irradiation are affective parameters for dye degradation processes.

Stability as well as recoverability of the nanocomposites are important subjects in the catalytic field. They have magnetic treatment and were swiftly segregated through the external magnet and after washing with distilled water reused. The recoverability test for the $Mn_3O_4/g\text{-}C_3N_4$ and $Ag_2MnO_4/g\text{-}C_3N_4$ nanocomposites was surveyed in degradation of MB and MO dyes, which were found to be reusable up to five and three cycles, respectively, with negligible loss in their catalytic activity (Fig. 11). FE-SEM images of the reused $Mn_3O_4/g\text{-}C_3N_4$ and $Ag_2MnO_4/g\text{-}C_3N_4$ nanocomposites for sonodegradation of MB dye are shown in Fig. 12. It can be seen that no remarkable change in the surface morphology of these robust catalysts was observed.

To exhibit the fascinating potential of the synthesized compounds in the area of the photocatalytic degradation process of dyes, the obtained results in this study have been compared with other reports in the literature. As the data in Table 2 show, $Mn_3O_4/g\text{-}C_3N_4$ and $Ag_2MnO_4/g\text{-}C_3N_4$ nanocomposites are comparable or superior to the reported procedures with respect to reaction time, temperature, degradation efficiency, or irradiation source. Both nanocomposites are suitable catalysts for sonodegradation of MB dye and $Mn_3O_4/g\text{-}C_3N_4$

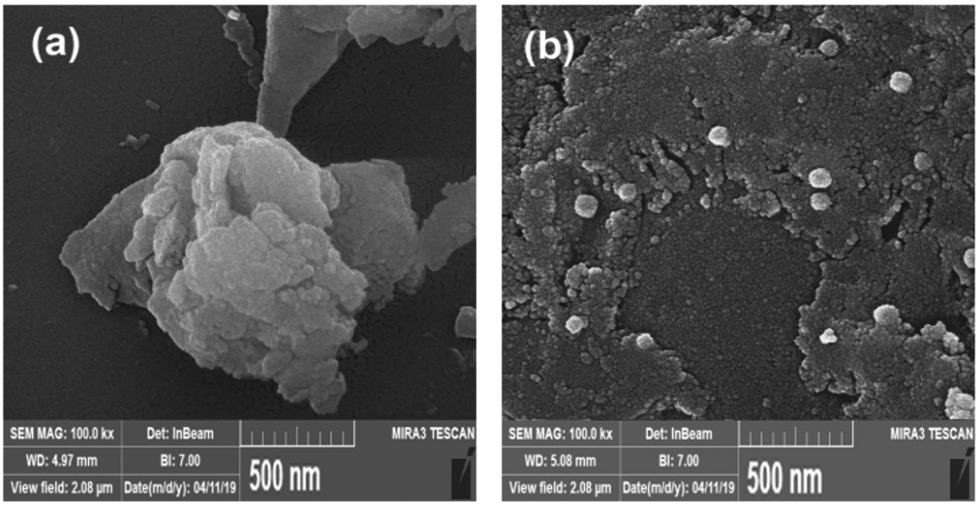


Fig. 12 — FE-SEM images of $Mn_3O_4$/*g*-$C_3N_4$ (a) and $Ag_2MnO_4$/*g*-$C_3N_4$ (b) nanocomposites for sonodegradation of MB dye after five cycles

nanocomposite is preferentially for sonodegradation of MO dye. Degradation efficiency of dyes can depend on shape, morphology, temperature, type of catalyst and dye as well as irradiation source. Ultrasonic irradiation can able destroy different organic dyes in short time with favorable efficiency. The utilization of this source is safe, easy, simple, and low-cost. The present investigation provides a new viewpoint in the degradation of organic dyes under ultrasonic irradiation in short time and proper efficiency.

## Conclusion

In summary, $Mn_3O_4$/*g*-$C_3N_4$ and $Ag_2MnO_4$/*g*-$C_3N_4$ nanocomposites, less than 50 nm in size, have been well synthesized. By coupling of $Mn_3O_4$ and $Ag_2MnO_4$ with *g*-$C_3N_4$, we expected to restrict fast recombination of electron-hole pairs in *g*-$C_3N_4$, as one of the most important reasons for its poor photocatalytic behaviour. Based on the experimental results, introduction of $Mn_3O_4$ and $Ag_2MnO_4$ into *g*-$C_3N_4$-cites could efficiently improve its photocatalytic performance and the obtained $Mn_3O_4$/*g*-$C_3N_4$ and $Ag_2MnO_4$/*g*-$C_3N_4$ nanocomposites with moderate band gap (ca. 3.6 eV) and strong oxidation power of valence band holes can be regarded as promising materials for photocatalysis application. The organic dyes were degraded over these nanocomposites under solar and ultrasound irradiation, the latter being suggestive of higher degrees of degradation in lower times, due to cavitation phenomenon. In this context, $Mn_3O_4$/*g*-$C_3N_4$ was much more active than $Ag_2MnO_4$/*g*-$C_3N_4$ in similar reaction conditions. Separation of the superparamagnetic sonocatalysts could be easily achieved using an external magnetic field and the recovered catalysts reused several times.

## Acknowledgements

The authors gratefully acknowledge Shahrekord University and Research Institute of Petroleum Industry for their financial support of this work.

## References

1 Liebing J, *Ann Pharm*, 10 (1834) 1.
2 Kumar A, Thakur P R, Sharma1 G, Naushad M, Rana A, Mola G T & Stadler F J, *Environ Chem Lett*, 17 (2019) 655.
3 Cui Y, Li M, Wang H, Yang C, Meng S & Chen F, *Sep Purif Technol*, 199 (2018) 251.
4 Li Y B, Zhang H M, Liu P R, Wang D, Li Y & Zhao H J, *Small*, 9 (2013) 3336.
5 Obregón S & Colón G, *Appl Catal B*, 144 (2014) 775.
6 Bayrama O, İgman E, Guney H & Simsek O, *Superlattices Microstruct*, 128 (2019) 212.
7 Gyrdasova O I, Sycheva N S, Baklanova I V, Buldakova L Y, Yanchenko M Y, Nefedova K V & Krasil'nikov V N, *J Mater Sci Mater Electron*, 30 (2019) 8820.
8 Molla A, Li Y, Mandal B, Kang S G, Hur S H & Chung J S, *Appl Surf Sci*, 464 (2019) 170.
9 Meti S, Rahman M R, Ahmad M I & Bhat K U, *Appl Surf Sci*, 451 (2018) 67.
10 Parvanak B K, Tohidiyan Z, Shahsanaei H A, Lorigooini Z & Fadavi A H, *Inorg Chem Commun*, 122 (2020) 108206.
11 Parvanak B K, Tohidiyan Z, Lorigooini Z, Hamidifar Z & Eskandari M M, *IET Nanobiotechnol*, 15 (2021) 197.
12 Ebrahimipour S Y, Sheikhshoaie I, Castro J, Dušek M, Tohidiyan Z, Eigner V A & Khaleghie M, *RSC Adv*, 5 (2015) 95104.
13 Kamali F, Eskandari M M, Rashidi A, Baghalha M, Hassanisadi M & Hamzehlouyan T, *J Hazard Mater*, 364 (2019) 218.

14 Klug H P & Alexander L E, *X-Ray Diffraction Procedures*: *For Polycrystalline and Amorphous Materials*, 2nd Edn., (Wiley, Inc., New York), 1974, p. 992.
15 Egekenze R N, Gultneh Y & Butcher R, *Inorg Chim Acta*, 478 (2018) 232.
16 Babasaheb B S, Gavade N L, Shinde H, Mahajan P G, Lee K H, Mane N, Deshmukh A, Garadkar K M & Bhuse V M, *ACS Appl Nano Mater*, 1 (2018) 4682.
17 Liu Z N, Xu K L, Sun H & Yin S Y, *Small*, 11 (2015) 2182.
18 Vázquez O A, Redón R, Rodríguez G G, Mata Z M E, Leal F M, Fernández O A L & Saniger J M, *J Colloid Interface Sci*, 291 (2005) 175.
19 Boyero J M, Fernández E L, Gallardo A J M, Ruano R C, Sánchez V E & Pérez E B, *Int J Inorg Mater*, 3 (2001) 889.
20 Brunold T C & Güdel H U, *Inorg Chem*, *36 (*1997)1946.
21 Parvanak B K, Tohidiyan Z, Fadavi A, Eskandari M M & Shahsanaei H A, *ChemistrySelect*, 4 (2019) 7734.
22 Xie H, Dong J, Duan J, Hou J, Ai S & Li X, *Sens Actuat B Chem*, 278 (2019) 147.
23 Xia S H, Zhang L, Pan G, Qian P & Ni Z H, *Phys Chem Chem Phys*, 17 (2015) 5348.
24 Parvanak B K, Tohidiyan Z, Hamidifar Z & Eskandari M M, *Indian J Chem Technol*, 29 (2022) 279.
25 Banat F, Asheh S A, Rawashdeh M A & Nusair M, *Desalination*, 181 (2005) 225.
26 Zheng X, Zhang D, Gaob Y, Wu Y, Liu Q & Zhu X, *Inorg Chem Commun*, 110 (2019) 107589.
27 Yu C, He H, Zhou W, Liu Z & Wei L, *Sep Purif Technol*, 217 (2019) 137.
28 Jiang Y, Liu P, Tian S, Liu Y, Peng Z, Li F, Ni L & Liu Z, *J Taiwan Inst Chem Eng*, 78 (2017) 517.
29 Wang C, Cao M, Wang P & Ao Y, *Mater Lett*, 108 (2013) 336.
30 Dom R, Subasri R, Radha K & Borse P H, *Solid State Commun*, 151 (2011) 470.
31 Sheikhshoaie I, Ramezanpour S & Khatamian M, *J Mol Liq*, 238 (2017) 248.
32 Gnanasekaran L, Hemamalini R, Saravanan R, Ravichandran K, Gracia F, Agarwal S & Gupta V K, *J Photochem Photobiol B*, 173 (2017) 43.
33 Nirumand L, Farhadi S, Zabardasti A & Khataee A, *Ultrason Sonochem*, 42 (2018) 647.
34 Bai Z, Sun B, Fan N, Ju Z, Li M, Xu L & Qian Y, *Chem Eur J*, 18 (2012) 5319.